Two-phase flow: structure, upscaling, and consequences for macroscopic transport properties

Renaud Toussaint, Knut Jørgen Måløy, Yves Méheust, Grunde Løvoll, Mihailo Jankov, Gerhard Schäfer, Jean Schmittbuhl

Two-phase flow: structure, upscaling, and consequences for macroscopic transport properties

R. Toussaint[1,6], K.J. Måløy[2,6], Y. Méheust[3,6], G. Løvoll[2, 4], M. Jankov[2], G. Schäfer[4], J. Schmittbuhl[1]

(1) IPGS, CNRS, University of Strasbourg, Strasbourg (France)
(2) Physics Department, University of Oslo, Oslo (Norway)
(3) Géosciences Rennes, University of Rennes 1, Rennes (France)
(4) Det Norske Veritas AS, Research and Innovation, Høvik (Norway)
(5) LHYGES, CNRS, University of Strasbourg, Strasbourg (France)
(6) Centre for Advanced Study, Centre for Advanced Study at The Norwegian Academy of Science and Letters, Oslo (Norway)

January 13, 2012

Abstract

In disordered porous media, two-phase flow of immiscible fluids (biphasic flow) is organized in patterns that sometimes exhibit fractal geometries over a range of length scales, depending on the capillary, gravitational and viscous forces at play. These forces, as well as the boundary conditions, also determine whether the flow leads to the appearance of fingering pathways, i.e., unstable flow, or not. We present here a short review of these aspects, focusing on drainage and summarizing when these flows are expected to be stable or not, what fractal dimensions can be expected, and in which range of scales. We base our review on experimental studies performed in two-dimensional Hele-Shaw cells, or addressing three dimensional porous media by use of several imaging techniques. We first present configurations in which solely capillary forces and gravity play a role. Next, we review configurations in which capillarity and viscosity are the main forces at play. Eventually, we examine how the microscopic geometry of the fluid clusters affects the macroscopic transport properties. An example of such an upscaling is illustrated in detail: For air invasion in a mono-layer glass-bead cell, the fractal dimension of the flow structures and the associated scale-ranges, are shown to depend on the displacement velocity. This controls the relationship between saturation and the pressure difference between the two phases at the macroscopic scale. We provide in this case expressions for dynamic capillary pressure and residual fluid phase saturations.

1 Introduction

The physics of two phase flows in porous media is a complex and rich topic, with obvious applications to the hydraulics of the vadoze zone, be it water infiltration, its evaporation, or the transport of Dense Non-aqueous Phase Liquids (DNAPL) down to the aquifers (Dridi et al., 2009). Hydrogeologists and soil scientists aim at relating volumetric flow, pressure head, and water content at the Darcy scale, which is a meso-scale above which the medium and the flow are described by continuous mathematical fields. They also need to predict the front displacement of the injected fluids, its localizing or non localizing character, and the fluid mass distribution behind it. The basic laws of multiphase flows treated at mesoscopic scale as a continuum require a closure of simultaneous flow according to Darcy's law. A key point of this closure is a functional relation between the capillary pressure and (water) saturation in the form of retention curves; another key point in the dependence of the relative permeabilities on saturation.

The physics community has been mostly concerned with characterizing and understanding flow structures/patterns from the pore scale and up. These structures and processes have a major impact on the retention curves (see e.g. review by Blunt (2001)). Notably, viscous fingering may have strong influence on retention curves, resulting in dynamic saturation–pressure curves in porous media as we will show in section 4 below.

These flow structures can vary from compact to ramified and fractal (Lenormand et al., 1988; 1989; Måløy et al., 1985; Méheust et al., 2002; Sandnes et al., 2011; Holtzman and Juanes, 2010). One major issue is to simplify this complexity by keeping just enough information to describe the relevant physics at the relevant scale for the flow considered, without discarding

essential information. For example, the simple invasion percolation model is sufficient to model the flow structure obtained under slow drainage conditions.

The fact that such simple models can describe simple features of complex systems arises from the property of universality in critical states: many physical dynamic systems, governed by a competition of simple forces with a disorder in thresholds, are in the vicinity of so-called critical points in statistical physics, as discussed e.g. by Domb (1996) or Feder (1988): these are characterized by scale invariance over some ranges, fractal dimensions, and by critical exponents precising how characteristic lengths that limit the fractal ranges depend on the system size or driving speed. An interesting aspect of such critical points is that the corresponding exponents and fractal dimensions do not depend on the small scale details of the system, but are controled by how the systems are invariant under some form of upscaling. Consequently many systems differing at small scale are characterized by the same critical exponents: they are said to belong to the same universality class. This allows to describe complex systems using sometimes simple computer models.

The porous body of a piece of soil or rock consists of pores and fracture networks of different length scales and shapes, whose permeability presents large spatial variations. These structures can be correlated at large scale (see e.g. Brown, 1995; Zimmerman and Bodvarsson, 1996; Méheust and Schmittbuhl 2003, Neuville et al. 2010a) or present a finite correlation length (Neuville et al. 2010b). The variations in permeability results in flow channeling (see e.g. Brown, 1987; 1995, Drazer and Koplik, 2002, Méheust and Schmittbuhl 2000, 2001, 2003, Neuville et al., 2010a, 2011a, 2011b, 2011c) and a potential permeability anisotropy (Méheust and Schmittbuhl 2000, 2001). In general the soil/rock is a dynamic medium where the porosity can be modified by the fluids involved due to chemical reactions and desorption/adsorption

77 mechanisms (Szymczak and Ladd, 2011), in addition to the fluid pressure and the mechanical
78 stress acting on the porous medium (Johnsen et al., 2006; Goren et al., 2010; 2011). The
79 chemical composition and nano/micro structure of the rock further decides the wetting properties
80 of the fluids which is crucial for the capillary front advancement in two-phase flow. For
81 example, when a fluid with high viscosity is displaced in a porous medium by a fluid with a
82 lower viscosity, the displacing fluid tends to channel through the paths of lower flow resistance,
83 thereby forming pronounced fingers. The physical properties of the fluids play an important
84 practical role on natural flows: e.g., in soil and groundwater, the identification of pollution
85 sources is difficult due to the fact that organic pollutants can rapidly migrate down to the bottom
86 of the aquifer and/or along paths different from the water (Benremita and Schäfer, 2003).
87 In addition, when the porous medium is deformable, branching structures can be observed with
88 transitions to fracturing of the porous medium (Lemaire et al., 1993; Cheng et al., 2008; Sandnes
89 et al., 2011; Holtzman and Juanes, 2010; Chevalier et al., 2009; Johnsen et al., 2006; Varas et al.,
90 2011) or formation of fingers, channels or bubbles in it (Johnsen et al., 2006; 2007; 2008; Kong
91 et al., 2011; Vinningland et al., 2007a; 2007b, 2010, 2011; Niebling et al., 2010a; 2010b).
92 In this review we will address the detailed structure and dynamics of two phase flow in
93 fixed and disordered porous media based on pore scale experiments. We will limit the discussion
94 mostly to drainage, i.e. to situations where a non wetting fluid displaces a wetting one - even
95 though imbibition, where a wetting fluid invades a non wetting one, is of equal practical
96 importance. The discussion will be limited to media that are isotropic and homogeneous at large
97 scales, and to cases where chemical reactions and adsorption or desorption between the fluids
98 and the porous medium can be neglected. The structures of clusters of the moving fluid and the
99 dynamics of drainage in porous media depend on several parameters like the density difference,

100 the surface tension, the wetting properties, the viscosities and the flow rates of the fluids
101 involved. The various forces at play dominate on different length scales and their interplay give
102 rise to separate scaling regimes. Up-scaling, which consists in relating the pore scale description
103 to properties defined at the Darcy scale or even at the macroscopic scale, is a central topic within
104 hydrology and petroleum engineering.

105 Only by understanding the scaling of the structures and dynamics within each regime,
106 and the crossover lengths involved, it is possible to perform up-scaling. The structures involved
107 are typically fractal within some scaling range; their fractal dimension depends on length scales,
108 and often result from fluctuations occurring at smaller scales. At the end of this short review we
109 provide an example of upscaling of recent experimental data; the experiments in question were
110 aimed at studying the crossover between capillary and viscous fingering in a quasi two–
111 dimensional (monolayer) porous medium.

112 This review summarizes the results of a series of works, published mostly in Physics
113 journals, that are of interest to model flow in the vadose zone, or in general in hydrology. We
114 will also illustrate on simple examples what type of microstructure and what properties of
115 fingering of the flow control upscaling and the dynamic dependence of macroscopic capillary
116 pressure on microscopic flow.

117

118 ## 2 Capillary and gravitational effects

119

120 When drainage is performed in the limit of infinitely slow displacement velocities, the
121 pressure drop accross the porous medium is controlled by the capillary pressure drop accross the
122 interface between the two fluids. The criterion for advancement of the interface into a given pore

is that the capillary pressure drop is larger than the capillary pressure threshold needed to invade the pore neck that separates that pore from the already-invaded adjacent pore. The value of the capillary pressure threshold fluctuates from pore neck to pore neck, with a distribution function determined by the geometry of the porous medium. In the case of zero gravity or for a horizontal 2D porous medium, the next pore throat /neck to be invaded will be, among the pores that touch the interface, the one whose pore throat has the smallest capillary pressure threshold. This idea is the basis of the invasion percolation algorithm (de Gennes and Guyon, 1978; Chandler et al., 1982; Wilkinson and Willemsen, 1983) where random numbers representing the capillary pressure threshold values are distributed on a lattice and where the front is moved at each time step at the location along the interface corresponding to the smallest threshold value. The fact that the fluid front always moves at the most easily invaded pore neck and nowhere else is actually not always true in real flows, even if it is a good approximation. What drives the advancement of the front is the capillary pressure build-up in the fluid. The capillary pressure will not relax immediately after invasion of a new pore but is controlled by a back contraction of the fluid interface. This is the reason for the so called Haines jumps which may lead to invasion of several pores in one jump (Haines, 1930; Måløy et al., 1992; Furuberg et al., 1996).

When the displaced fluid is incompressible (or lowly compressible), trapping takes place. Trapping is very important in two dimensions (2D) (Wilkinson and Willemsen, 1983) but much less significant in three dimensions (3D). Experiments addressing capillary fingering in 2D model systems were first performed by Lenormand et al. (1988; 1989) who found a mass fractal dimension of the invaded structures equal to $D_c = 1.83$, which is consistent with the results of numerical simulations based on invasion percolation (in the version of the model allowing trapping of the invaded fluid) (Wilkinson and Willemsen, 1983). In 3D, several experiments

146 have been performed (Chuoke et al., 1959; Paterson et al., 1984a; 1984b; Chen et al., 1992;
147 Frette et al.1994; Hou et al., 2009; Mandava et al., 1990; Nsir et al., 2011; Yan et al., 2012). The
148 fractal dimension found at small scale (between 2.0 and 2.6) is compatible with the dimension
149 $D = 2.5$ found in three dimensional invasion percolation models (Wilkinson and Willemsen,
150 1983).
151 Even though the capillary fingering structure is fractal, in practice it is well described by a fractal
152 dimension only within a window of length scales ranging from the pore size up to a crossover
153 length on a larger scale. In the case where the density difference between the two fluids is
154 different from zero, but where viscous forces are small compared to the others, this crossover
155 length corresponds to a scale at which the capillary threshold fluctuations become of the same
156 order of magnitude as the difference in hydrostatic pressure drop between the two fluids. This
157 means that the crossover will always occur when the fluid structures become large enough.
158 When a lighter fluid is displacing a heavier one from above at a slow flow rate resulting in low
159 viscous forces, a stable displacement is observed. In this case, the displacing fluid does not finger
160 its way through the displaced fluid; the crossover length sets the width of the rough interface
161 between the two fluids (Birovljev et al., 1991; Méheust et al., 2002; Løvoll et al., 2005), parallel
162 to the average flow direction .
163 Gravitational effects can easily be accounted for in the invasion percolation model by mapping
164 the system onto a problem where the capillary threshold values are modified linearly by the
165 hydrostatic pressure difference between the two fluids (Wilkinson, 1984; Birovljev et
166 al., 1991; Auradou et al., 1999). By using this theory of percolation in a gradient, Wilkinson
167 (1984) predicted theoretically the scaling of the front width ξ observed in a gravitational field as

168 $$\xi / a \propto Bo^{\frac{-\nu}{\nu+1}}, \qquad (1)$$

where the Bond number $Bo = \Delta\rho g a^2/\gamma$ is the ratio of the difference of the hydrostatic pressure drops in the two fluids on the length scale of a single pore to the capillary pressure drop, and ν is the critical exponent associated to correlation length divergence in percolation theory (ν = 4/3 in 2D, Wilkinson (1984)). Here, $\Delta\rho$ is the density difference between the fluids, g the gravitational acceleration, a the characteristic pore size and γ the surface tension between the two fluids. Gravitationally-stabilized fluid fronts occurring during very slow two-dimensional drainage have been studied both experimentally and by computer simulations (Birovljev et al., 1991). The results were found consistent with the theoretical prediction of Wilkinson (1984). When a lighter fluid is injected into a heavier fluid from below (Frette et al., 1992; Birovljev et al., 1995; Wagner et al., 1997), gravitational fingering of the displacing fluid through the displaced fluid occurs; a scaling behavior consistent with Eq. (1) has also been found in this unstable case: the characteristic length scale ξ then corresponds to the width of the unstable gravitational fingers, perpendicularly to the average flow direction. The same simple mapping to invasion percolation as described above can also be performed in the case of slow displacement in a rough fracture joint filled with particles (Auradou et al., 1999).

When comparing systems with different capillary pressure threshold distributions, Eq.(1) needs to be modified. From the phenomenology of the invasion process that we have explained above, it is quite intuitive that a gravity - stabilized front in a porous medium presenting a narrow capillary noise (i.e. a narrow distribution of the capillary thresholds) will give a flatter front than a porous medium with a wide capillary noise. Instead of equation Eq. (1), it has therefore been suggested to take into account a dimensionless fluctuation number $F = \Delta\rho g a/W_t$, in which capillary fluctuations are accounted for in terms of the width W_t of the capillary pressure distribution (Auradou et al., 1999; Méheust et al., 2002). Experiments to check the dependence

of the displacement process on the capillary noise (W_t) are difficult, because controlling the distribution of threshold capillary pressures in the medium in a systematic way is not straightforward . These experiments therefore remain to be done.

3 Capillary and viscous effects

The crossover between capillary fingering and regimes for which viscous effects are dominant was first studied in the pioneering work of Lenormand (1988). He classified the different flow structures in a phase diagram depending on the viscosity contrast $M = \mu_i/\mu_d$ between the fluids and the capillary number $Ca = \Delta P_{\text{visc}}/\Delta P_{\text{cap}}$, which is the ratio of the characteristic viscous pressure drop at the pore scale to the capillary pressure drop. Here μ_i and μ_d are the viscosities of the injected and displaced fluid, respectively. From the Darcy equation, the capillary number can be evaluated as

$$Ca = \frac{\Delta P_{\text{visc}}}{\Delta P_{\text{cap}}} = \frac{a\nabla P_{\text{visc}}}{\gamma/a} = \frac{\mu a^2 v}{\kappa\gamma}. \qquad (2)$$

where γ is the surface tension, a the characteristic pore size, ΔP_{visc} is the viscous pressure drop at pore scale a, evaluated from the viscous pressure gradient ∇P_{visc}, κ the intrinsic permeability of the medium, v the seepage velocity associated to the imposed flow rate of the displaced fluid, μ the viscosity of the most viscous fluid, and γ/a the typical capillary pressure drop accross the interface. Lenormand identified three flow regimes: (i) stable displacement, for which the interface roughness is not larger than one linear pore size, (ii) capillary fingering, which we have discussed in section 2, and (iii) viscous fingering, which occurs when large scale fingers of the

displacing fluid develop inside a more viscous defending fluid, resulting in a much faster breakthrough of the displacing fluid. It is important to keep in mind that the observed structures will depend on the length scale considered. For large systems it is therefore not meaningful to talk about a sharp transition in a phase diagram between capillary and viscous fingering, because one will always have both structures present, i.e. capillary fingering on small length scales, and either viscous fingering or stable displacement on large length scales. When the two fluids involved have different viscosities, the viscous pressure drop between two points along the fluid interface will typically be different in the two fluids. This viscosity contrast will produce a change in the capillary pressure along the fluid interface, therefore playing a role similar to that of density contrasts in the presence of a gravitational field (see section 2). At sufficiently large length scales, the difference in viscous pressure drop between the two sides of the interface will become larger than the typical fluctuations in capillary pressure threshold. This means that at sufficiently large length scales, and thus for a sufficient large system, viscous pressure drops, rather than capillary forces associated to random capillary thresholds, determine the most likely invaded pores; consequently, viscous fingering will always dominate at sufficiently large scales when a viscous fluid is injected into another more viscous fluid. At these large scales, and in the absence of a stabilizing gravitational effects, two-dimensional flows exhibit tree-like branched displacement structures with a mass fractal dimension $D_v = 1.6$ (Måløy et al., 1985). The fractal dimension of the front, or growing hull, was found experimentally to be around 1, close to the growing interface dimension in DLA models (Feder; 1988).

Méheust et al. (2002) have introduced a generalized fluctuation number

$$F = \frac{\Delta\rho g a - \frac{a\mu v}{\kappa}}{W_t} \qquad (3)$$

which is the ratio of the typical total pressure drop in the fluids over one pore, including both viscous and gravitational pressure drops, to the width of the capillary pressure threshold distribution W_t. The experiments by Méheust et al. (2002), identical to those by Birovljev et al. (1991) but performed at larger flow rates and therefore under significant viscous effects, showed that the characteristic width of the rough interface parallel to the macroscopic flow could be characterized with the fluctuation number according to an equation analog to Eq.(1):

$$\xi/a \propto F^{\frac{-\nu}{\nu+1}} \tag{4}$$

where the exponent $\nu/(1+\nu) = 4/7$ is consistent with percolation theory ($\nu = 4/3$) in 2D. Since the viscous pressure field is not homogeneous like the gravitational field, this result is not obvious. Note that in this case ξ can be interpreted as the length scale at which the sum of the viscous and gravitational pressure drop becomes of the same order of magnitude as the spatial fluctuations of the capillary pressure threshold. In terms of fluid-fluid interface, ξ corresponds to the crossover scale between capillary fingering structures at small scale and the stabilized structure, which is linear (dimension 1) at large scales. When the displacement is large enough for viscous forces to play a role, the fractal dimension typical of viscous fingering structures is also seen at intermediate scales (Méheust et al., 2002). Even in the case where the two fluids involved have the same viscosity, the width of the front was found to be consistent with Eq.(4) (Frette et al.,1997). As observed in the experiments of Frette et al. (1997), the effect of trapping turns out, at least in two dimensions, to be of central importance. The trapped islands result in a decrease in the relative permeability of the invaded fluid, which is equivalent to having a fluid with a higher viscosity (as was shown by Frette et al. (1997) by the comparison to simulations allowing trapping or not, with growth along the whole external perimeter of the invader or restricted to the hull). This is the effect responsible for the well-known decreasing dependence of

a soil's matric potential on its water content. This result is consistent with the scaling relation Eq.(4), which is expected from theoretical arguments for percolation in a stabilizing gradient (Xu et al., 1998; Wilkinson, 1984; Lenormand, 1989). Note that other scaling relations have been derived theoretically and observed experimentally by other authors, as reported by Wu et al. (1998). As mentioned previously, when a viscous fluid is injected into a 2D medium filled with a more viscous fluid, viscous fingers occur. The scaling of the finger width was studied experimentally by Løvoll et al. (2004) and Toussaint et al. (2005). The measurements were found to be consistent with a scaling law in the form

$$\xi/a \propto \mathrm{Ca}^{-1} \tag{5}$$

This result is different from the scaling laws that can be explained from the theory of percolation in a gradient, as observed from stabilizing viscous or gravitational forces. In the experiments of Løvoll et al. (2004) and Toussaint et al. (2005), contrarily to what happens in a pressure field arising from gravitational effects (as in Méheust et al. (2002)), the viscous pressure field is highly inhomogeneous, constant in front of the fingers, and screened by the fingers behind the invasion front (i.e. the pressure gradient concentrates around the finger tips and decays behind the finger tips, in the stagnant zones). This may explain why the behaviour expected from percolation in a gradient is not observed, but a rather simpler one instead. Note however that scaling laws based on the theory of percolation in a gradient are still expected for some types of unstable flows (Xu et al. 1998).

The scaling law, Eq. (5), can be explained from a simple mean field argument: consider an approximation for the pressure field for which the pressure gradient ∇P is homogeneous around the mobile sites at the boundary between the two fluids. Let us consider two of these sites, separated by a distance l along the direction of ∇P; the difference between the drops in

viscous pressure across the interface at the two sites is $l\nabla P \approx l\mathrm{Ca}\gamma/a^2$. This relation holds not only when the viscosity of one fluid can be neglected with respect to that of the other one (for example, for air and water), in which case a non-zero viscous pressure difference between the two sites occurs in the defending liquid only, and the definition of the capillary number is given by Eq. (2). It also holds in the general case of two viscous fluids, in which case the capillary number can be defined from Eq. (2) by replacing the viscous pressure difference by the difference in the viscous pressure drop across the interface at the two sites, or equivalently by the differential viscous pressure drop $|\Delta P_v^{(i)} - \Delta P_v^{(d)}|$, where the $|\Delta P_v|$ are viscous pressures difference between the two sites in each of the phases, the superscript $^{(i)}$ and $^{(d)}$ denoting respectively the invading- and defending- phase. If the differential viscous pressure difference between these two sites exceeds the characteristic random fluctuations of the capillary pressure threshold from one pore throat to another along the interface, then the viscous pressure field is dominant in determining at which of the two points considered new pores are going to be invaded. On the contrary, if the random fluctuations of capillary threshold exceed the differential viscous pressure drop between the two points, then this random pressure difference component dominates. Assuming that its magnitude W_t is of the same order as the average capillary pressure value, γ/a we conclude that capillary effects are expected to dominate for scales l such that $l\mathrm{Ca}\gamma/a^2 < \gamma/a$, whereas viscous effects will dominate for larger scales, such that $l\mathrm{Ca}\gamma/a^2 > \gamma/a$: this explains the observed cross over scale $\xi = a/\mathrm{Ca}$ between the structures characteristic of capillary fingering and those characteristic of viscous fingering. Using a pore-scale simulation where they can tune capillary noise, Holtzman and Juanes (2010) determined a phase diagram of the displacement regime (capillary or viscous fingering) as a function of capillary noise and capillary number, and observed the same crossover, which they explained in a similar manner,

304 only expressing the prefactor for the scaling law of the crossover scale in terms of typical
305 capillary pressure threshold fluctuations rather than in terms of the mean capillary pressure
306 threshold (that is, they did not assume that $W_t \approx \gamma/a$).
307
308 # 4 An example of upscaling from capillary to viscous fingering
309
310 In many situations of non-miscible biphasic flow in porous media, the flow gets
311 organized in fingering structures (preferential paths); in these unstable configurations, the fluids
312 arrange in fractal geometries with nontrivial fractal dimensions depending on the observation
313 scale, and the scale range over which each dimension is observed depends on the imposed
314 boundary conditions (such as the macroscopic fluxes). This microscopic structuration has far
315 reaching consequences for the upscaled relationships between, for example, saturation and the
316 pressure difference between the two phases.
317 An example of such a situation has been mentioned briefly earlier in this review: if
318 gravity is negligible, only capillarity and viscosity play a role on the flow; when a fluid of lower
319 viscosity displaces a more viscous one, the fluid-fluid interface is unstable due to viscous
320 pressure gradients increasing at the most advanced parts of the invader, so that fingers naturally
321 arise. The development of such an interface instability occuring during drainage was studied
322 optically in Hele Shaw cells, at several controlled injection rates (Løvoll et al.2004; Toussaint et
323 al.2005). Air was injected into an artifical porous medium composed of a monolayer of immobile
324 glass beads sandwiched between two glass plates, and initially filled with a wetting dyed
325 glycerol-water solution. The Hele-Shaw cell dimensions were denoted $L \times W \times H$, $H = 1$ mm
326 being the cell thickness as well as the typical glass bead diameter; flow was imposed along the

length L, with impermeable lateral boundaries defining a channel of width W (see Fig. 1). An occupancy (also termed occupation probability) was defined in the reference frame moving at the average finger speed between the system boundary; in that referential, the invasion structure is seen as a finger fluctuating during the experiment behind its stationary tip: for each point in this reference frame, the proportion of the time where this point is occupied by the invading fluid is a measure of the occupancy. It was shown in these experiments that the pathway of the air, defined as the locations where the occupancy probability exceeds half its maximum value, was a finger of width λW positioned in the centre of the channel, with $\lambda = 0.4$. This was attributed to a similarity between the process of selection of the pore throats to be invaded and a Dielectric Breakdown Model of exponent 2 (Niemeyer et al., 1984), that is, a growth process in which the growth velocity is proportional to the gradient of the driving effect to the power of 2. The presence of a disorder in capillary threshold turns out to be important to enforce a boundary condition analogous to a growth probability along the invader proportional to $[(P - P_{air})/a]^2$, with a field P satisfying Laplace equation due to mass conservation: This result was justified theoretically by computing the average invasion speed taking into account the width of the capillary threshold distribution (Toussaint et al.,2005). This type of invasion structure is illustrated in Fig. 1.

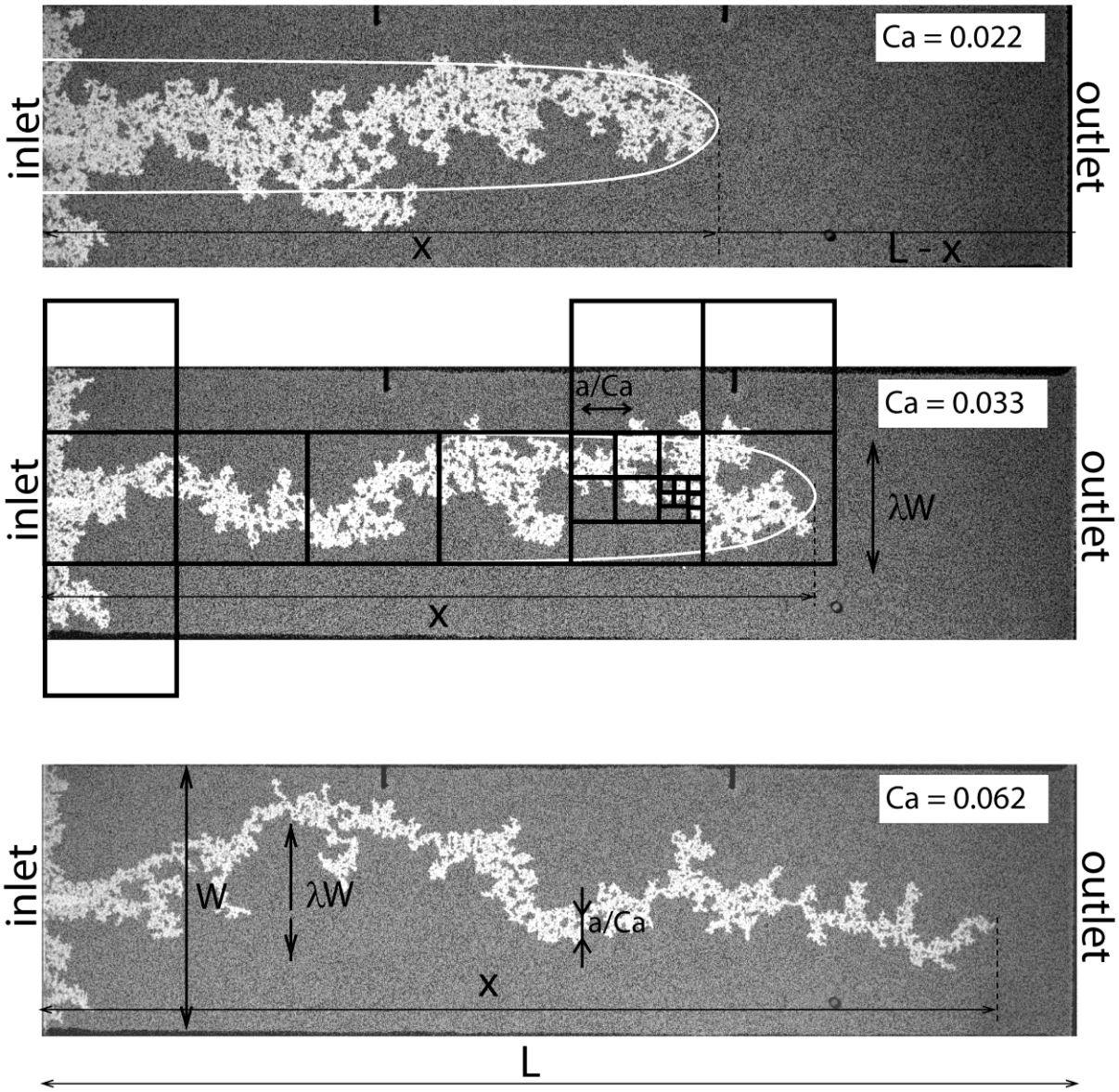

Figure 1: Invasion structure of a fluid with a low viscosity (white) into a much more viscous one (dark grey) during drainage in an artificial 2D porous medium of width W and extent L, at three different extraction speeds. The position of the invasion tip is denoted x. Characteristic crossover scales between fractal regimes, λW and a/Ca, separate a straight finger structure, a viscous fingering geometry, and a capillary fingering geometry, down to the pore scale a. The black square of various dimensions in the central figure illustrate the types of boxes used in the box counting measure of the fractal dimension: for boxes of a certain side size *l*, one counts the number of boxes *N(l)* needed to cover the structure. This is done for various sizes, from system size down to pixel size. The scaling of this number as function of the size, $N(l) \sim l^{-D}$ defines the mass fractal dimension *D*. The sizes *W* and *a/Ca* turn out to be the limits of scale-ranges with well defined fractal dimensions: $D = 1.00$ above W, $D_v = 1.60$ between W and a/Ca, and $D_c = 1.83$ below. Modified from Løvoll et al. (2011).

From approximations on the shape of the pressure around this finger, mostly controlled by the viscous pressure drop, one can derive an upscaled pressure-saturation relation (Løvoll et al.2010).

Indeed, the pressure presents to first order a linear viscous pressure drop from the tip of the invasion cluster, at position x, to the outlet of the system, at position L. Over the rest of the system, the pressure gradient is screened by the finger, rendering the pressure in the wetting fluid essentially constant at a value close to the sum of the air pressure and the entrance pressure γ/a. Hence, the pressure difference between the two phases, with a pressure in the wetting fluid P_w measured at the outlet, the one in the non wetting phase equal to the atmospheric pressure $P_{n.w.}$, and a correction to this entrance pressure, writes as

$$\Delta P^* = P_{n.w.} - P_{w.} - \gamma/a = (L-x)\nabla P \quad (6)$$

$$= (L-x)\Delta P_{\text{visc}}/a \quad (7)$$

$$= (L-x)\Delta P_{\text{cap}}\text{Ca}/a \quad (8)$$

$$= (L-x)\frac{\gamma \text{Ca}}{a^2} \quad (9)$$

where ΔP_{visc} and ΔP_{cap} are considered at the pore scale. Thus, there is a linear relationship between the viscous pressure drop accross the cell and the distance between the finger tip and the outlet.

In addition, the relationship between saturation and capillary number can be inferred from the fractal structure of the non-wetting invading fluid. At scales above the width λW, the finger is a linear structure of dimension 1. Between the scale λW and a/Ca, the structure has a viscous fingering geometry of fractal dimension $D_v = 1.60$ (Måløy et al.,1985; Løvoll et al.,2004). Between the crossover scale a/Ca and the pore scale a, the structure has a capillary

fingering geometry of fractal dimension $D_c = 1.83$. Hence, the total number of pores invaded by the non viscous fluid (n.v.f.) can be evaluated as a function of these fractal dimensions, the ratio of the finger length to its width, $x/(\lambda W)$, and the ratios of the latter length to the two others lengths, the crossover length and the pore size. This leads to:

$$N_{n.w.} = \frac{x}{\lambda W}\left(\frac{\lambda W}{a\mathrm{Ca}^{-1}}\right)^{D_v}\left(\frac{a\mathrm{Ca}^{-1}}{a}\right)^{D_c} \tag{10}$$

Together with the relationship between the total number of pores and the characteristic model dimensions,

$$N_{tot} = \frac{LW}{a^2} \tag{11}$$

and the relationship between the wetting phase and non-wetting phase saturation $S_{n.w.}$,

$$S_{n.w.} = 1 - S_{w.} = \frac{N_{n.w.}}{N_{tot}}, \tag{12}$$

Eq. (10) leads to

$$1 - S_{w.} = S_{n.w.} = \lambda^{D_v - 1}\left(\frac{a}{W}\right)^{2-D_v}\mathrm{Ca}^{D_v - D_c}\left(1 - \frac{a^2\Delta P^*}{\gamma L\mathrm{Ca}}\right) \tag{13}$$

This relationship allows to collapse all the pressure difference curves measured as a function of saturation in the set of experiments performed by Løvoll et al. (2010) onto a unique master curve for capillary numbers ranging from around 0.008 to 0.12. Note that the rescaled pressure $P^* = a^2\Delta P^*/(\gamma L\mathrm{Ca}) = (\Delta P^*/M)/(\Delta P_{visc}/a)$ is simply the ratio of the gradient in viscous pressure defined at the scale of the model to the gradient in viscous pressure defined at the pore

scale. Apart from the normalization by $\Delta P_{visc}/a$, it is nothing else than what is usually defined at the scale L of the experimental model as the capillary pressure. In other words, Eq. (13) defines the dependence on Darcy/seepage velocity of what is commonly denoted as dynamic capillary pressure, measured at scale L. This example shows how both viscous and capillary effects play a role in constraining the geometry of the invasion structures, resulting in a dynamic capillary pressure, as it is traditionally called (Hassanizadeh et al., 2002), that is simply due to the upscaling of the invasion structure, with only capillary and viscous effects seen at the REV scale, and without any dynamic capillary/wetting effects occuring at the pore scale.

Figures 2 and 3 illustrate respectively the raw measurements at several injection speeds and how Eq. (13) allows to collapse these curves of saturation versus pressure: with a reduced saturation $S^* = \lambda^{1-D_v}\left(a/W\right)^{-2+D_v}\mathrm{Ca}^{D_c-D_v}S_{n.w.}$ and the rescaled pressure $P' = a^2\Delta P^*/(\gamma L\mathrm{Ca}) = (\Delta P^*/M)/(\Delta P_{visc}/a)$, Eq. (13) predicts that $P' = 1 - S^*$, which is the theoretical straight line in Fig. 3. This is well followed by the experimental data collapse.

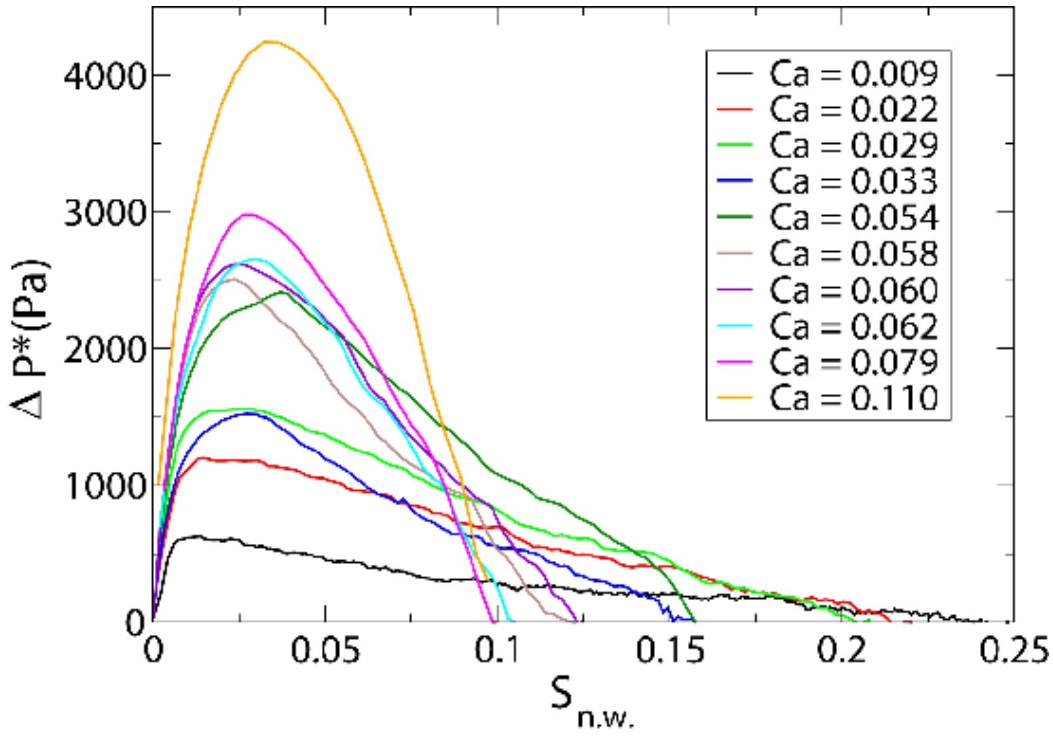

Figure 2: Dependence of the pressure difference between the two phases and the saturation of the invading fluid after removal of the average capillary pressure drop, $\Delta P^* = P_{n.w.} - P_{w.} - \gamma/a$, at different injection speeds. Adapted from Løvoll et al. (2011).

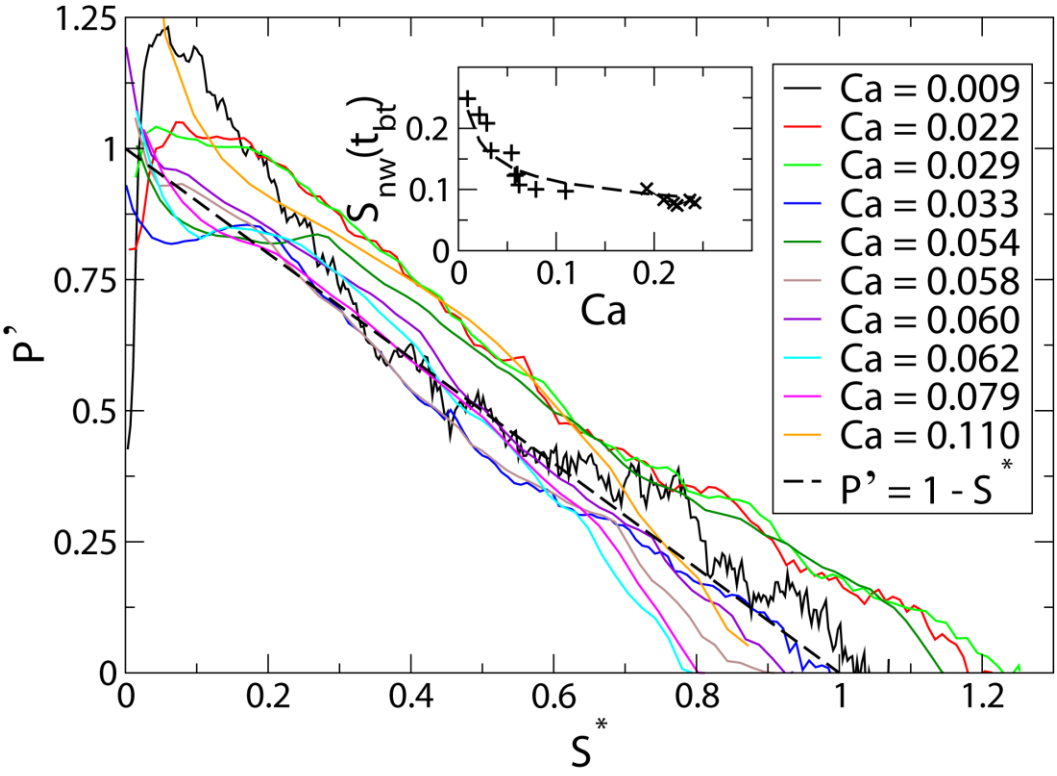

418

419 **Figure 3:** The collapse of the relationship between the reduced pressure difference
420 (between the two phases), $P' = a^2 \Delta P^* / (\gamma L \mathrm{Ca})$, and the reduced saturation of the invading fluid,
421 $S^* = \lambda^{1-D_v} (a/W)^{-2+D_v} \mathrm{Ca}^{D_c - D_v} S_{n.w.}$, at different injection speeds, shows the influence of the
422 structure on the upscaling. Note that plots corresponding to lower Ca values have been rescaled
423 more and therefore appear more noisy. Dashed curve: prediction. Inset: Residual saturation at
424 breakthrough. Adapted from Løvoll et al. (2011).

425

426 The viscous pressure drop accross the cell drops linearly as the finger progresses into the
427 cell, from a maximum value at the beginning of the invasion of $\gamma L \mathrm{Ca}/a^2$, down to 0 at
428 breakthrough of the invasion finger. In the previous equation, the wetting saturation is indeed
429 initially 1 as it should be at initial total saturation, but we also obtain the final and maximum

value of the residual wetting saturation as

$$1-S_{w.r.}=S_{n.w.r.}=\lambda^{D_V-1}\left(\frac{a}{W}\right)^{2-D_V}\mathrm{Ca}^{D_V-D_c}. \quad (14)$$

This relation between the residual saturation and the capillary number is indeed consistent with the observed residual saturations, as shown in the inset of Fig.3.

Besides the relation between saturation and the macroscopic pressure difference between the phases, other macroscopic relations can be obtained via upscaling, as e.g., in some situations, the relative permeability. For example, in other experiments where both fluids were injected at the same time, with both drainage and imbibition happening in the flow simultaneously, the trapped structures of wetting fluids were observed to be fractal up to a certain cutoff depending on the imposed flux (Tallakstad et al., 2009a; 2009b). A scaling law was observed for the relative permeability of wetting viscous fluid in these experiments, with an observed dependence on the imposed flux that can be expressed as $\kappa_{\mathrm{rel}} \propto \mathrm{Ca}^{-1/2}$. The upscaling explaining the cutoff and the structures allowed to explain this measured scaling law.

For the pure imbibition case, the macroscopic capillary pressure also presents a dynamic dependence: it was found by Stokes et al. (1986) and Weitz et al. (1987) that the fingering also occurs when the lower viscous fluid displaces the more viscous one, and that the finger width scales as $\mathrm{Ca}^{-1/2}$, a result that is still largely unexplained.

5 Conclusion

We have discussed the local flow structures that are observed experimentally during drainage in a disordered porous medium. When the viscosity constrast between the two fluids is

high (as for air displacing water), the flow structures are fractal, with a fractal dimension that depends on the observation scale. At small scales, capillary fingering exhibits a fractal dimension of 1.8 for two-dimensional media, and between 2 and 2.6 for three-dimensional media. At larger scales a branched structure characteristic of viscous fingering is seen, with a fractal dimension 1.6 for two-dimensional systems. The crossover between the two behaviors occurs at a length scale for which the differential viscous pressure drop equals the typical capillary pressure threshold in the medium. This means that for horizontal flow, unstable viscous fingering is always seen at large enough scales, even if the medium exhibits no permeability heterogeneities at the Darcy scale. From the definition of the crossover length, it follows that it scales as the inverse of the capillary number, which explains why experiments performed at a given experimental scale and at very slow flow rates have evidenced capillary fingering, while those performed at very large flow rates have evidenced viscous fingering. As for the effect of gravity, it can be to either destabilize or stabilize the interface, depending on which fluid is the densest. In the latter case, it acts against capillary effects and, when the displacing fluid is the most viscous, against the destabilizing viscous forces, resulting in an amplitude of the interface roughness that scales as a power law of the generalized fluctuation number (or generalized Bond number Bo – Ca, as introduced by Méheust et al. (2002)). In horizontal two-dimensional flows, viscous fingering is observed to occur up to another characteristic length that is a fixed fraction of the width of the medium. Upscaling of the local flow structures is possible once one knows the fractal dimensions typical of the flow regimes, and the relevant length scale range for each of them. We have given an example of how the measured capillary pressure can be related theoretically to water saturation, a relation that is confirmed by measurements. In that example, the capillary pressure measured at the scale of the experimental setup exhibits dynamic features,

i. e., a dependence on the flow rate, that is fully explained by the geometry of the upscaling, without any dynamic effects in the physical capillary pressure as defined at the pore/interface scale.

6 Acknowledgements

This work was supported by the CNRS through a french-norwegian PICS grant, the Alsace region through the REALISE program, and the Norwegian NFR.

References

Auradou H., K.J. Måløy, J. Schmittbuhl, A. Hansen, and D. Bideau. 1999. Competition between correlated buoyancy and uncorrelated capillary effects during drainage, Phys. Rev. E. 60:7224-7234.

Benremita H., G. Schäfer. 2003. Transfert du trichloréthylène en milieu poreux à partir d'un panache de vapeurs. C. R. Mecanique 331, 835-842.

Birovljev A., L. Furuberg, J. Feder, T. Jøssang, K.J. Måløy, and A. Aharony. 1991. Gravity invasion percolation in two dimensions: experiment and simulation. Phys. Rev. Lett. 67(5):584-587.

Birovljev A., G. Wagner, P. Meakin, J. Feder, and T. Jøssang. 1995. Migration and fragmentation of invasion percolation clusters in two-dimensional porous media. Phys.

Rev. E 51(6):5911-5915.

Blunt, M.J. 2001. Flow in porous media – pore-network model and multiphase flow. Current Opinion in Colloid and Interface Science. 6:197-207.

Brown, S. 1995. Simple mathematical model of a rough fracture. J. of Geoph. Res., 100(B4):5941-5952.

Brown, S. R. 1987. Fluid flow through rock joints: The effect of surface roughness. J. Geoph. Res., 92(B2):1337-1347.

Chandler R., J. Koplik, K. Lerman, and J.F. Willemsen. 1982. Capillary diplacement and percolation in porous media. J. Fluid Mech., 119:249-267.

Chen S., K.H. Kim, F. Qin, and A. T. Watson. 1992. Quantitative NMR imaging of multiphase flow in porous media. Mag. Res. Imaging 10(5):815-826.

Cheng, X., L. Xu, A. Patterson, H.M. Jaeger, and S.R. Nagel. 2008. Towards the zero-surface-tension limit in granular fingering instability. Nat. Phys. 4(3):234-237. doi:10.1038/nphys834.

Chevalier, C., A. Lindner, M. Leroux, and E. Clément. 2009. Morphodynamics during air injection into a confined granular suspension. J. Non-newtonian Fluid Mech. 158(1-3):63-72. doi:10.1016/j.jnnfm.2008.07.007.

Chuoke R. L., P. Van Meurs, and C. Van der Poel. 1959. The instability of slow, immiscible, viscous liquid-liquid displacement in permeable media, Trans. AIME 216:188-194.

de Gennes P.G., and E. Guyon. 1978. Lois generales pour l'injection d'un fluide dans un milieu

poreux aléatoire. J. Mec (France), 17:403-432.

Domb, C. 1996. The critical point – a historical introduction to the modern theory of critical phenomena. Taylor and Francis, London, Bristol.

Drazer, G., and J. Koplik. 2002. Transport in rough self-affine fractures. Phys. Rev. E, 66:026303.

Dridi, L., I. Pollet, O. Razakarisoa, and G. Schäfer. 2009. Characterisation of a DNAPL source zone in a porous aquifer using the partitioning interwell tracer test and an inverse modelling approach, J Cont. Hyd. 107(1-2):22-44.

Feder J. 1988. Fractals. Plenum Press, New York and London.

Frette V., J. Feder, T. Jøssang, P. Meakin, and K.J. Måløy. 1994. Fast, immiscible fluid-fluid displacement in three-dimensional porous media at finite viscosity contrast. Phys. Rev. E 50:2881-2890.

Frette V., J. Feder, T. Jøssang, and P. Meakin. 1992. Buoyancy-driven fluid migration in porous media. Phys. Rev. Lett. 68:3164-3167.

Frette O.I., K.J. Måløy, J. Schmittbuhl, and A. Hansen. 1997. Immiscible displacement in 2D porous media with a viscosity contrast equal to one. Phys. Rev. E. 55:2969-2975.

Furuberg L., K.J. Måløy, and J. Feder. 1996. Intermittent behavior in slow drainage. Phys. Rev. E 53:966-977.

Goren, L., E. Aharonov, D. Sparks, and R. Toussaint. 2010. Pore pressure evolution in deforming granular material: A general formulation and the infinitely stiff approximation.

J. Geophys. Res., 115(B09216), 2010. doi:10.1029/2009JB007191.

Goren, L., E. Aharonov, D. Sparks, and R. Toussaint. 2011. The Mechanical Coupling of Fluid-Filled Granular Material Under Shear. Pure Appl. Geophys. 168:2289-2323. DOI 10.1007/s00024-011-0320-4.

Haines W.B. 1930. Studies in the physical properties of soil. V. The hysteresis effect in capillary properties, and the modes of moisture distribution associated therewith. J. Agric. Sci. 20:97-116.

Hassanizadeh, S.M., M.A. Celia, and H.K. Dahle. 2002. Dynamic effect in the capillary pressure-saturation relationship and its impacts on unsaturated flow. Vadose Zone J. 1, 38–57.

Holtzman, R., and R. Juanes. 2010. Crossover from fingering to fracturing in deformable disordered media. Phys. Rev. E 82:046305.

Hou J., Z.Q. Li, S.K. Zhang, X.L. Cao, Q.J. Du, and X.W. Song. 2009. Computerized tomography study of the microscopic flow mechanism of polymer flooding, Transp. Porous Med. 79(3):407-418.

Johnsen, Ø., R. Toussaint, K.J. Måløy, and E.G. Flekkøy. 2006. Pattern formation during central air injection into granular materials confined in a circular Hele-Shaw cell. Phys. Rev. E 74:011301. doi:10.1103/PhysRevE.74.011301

Johnsen, Ø., R. Toussaint, K.J. Måløy, E.G. Flekkøy, and J. Schmittbuhl. 2007. Coupled air/granular flow in a linear Hele-Shaw cell", Phys. Rev. E 77:011301. doi:10.1103/PhysRevE.77.011301

Johnsen, Ø., C. Chevalier, A. Lindner, R. Toussaint, E. Clément, K.J. Måløy, E.G. Flekkøy, and J. Schmittbuhl. 2008. Decompaction and fluidization of a saturated and confined granular medium by injection of a viscous liquid or a gas. Phys. Rev. E 78:051302. doi:10.1103/PhysRevE.78.051302

Kong, X.Z. M. Holzner, F. Stauffer, and W. Kinzelbach. 2011. Time-resolved 3D visualization of air injection in a liquid-saturated refractive-index-matched porous medium. Exp. in fluids 50(6):1659-1670.doi:10.1007/s00348-010-1018-6.

Lemaire, E., Y. O. M. Abdelhaye, J. Larue, R. Benoit, P. Levitz, and H. van Damme. 1993. Pattern formation in noncohesive and cohesive granular media. Fractals 1: 968-976. doi:10.1142/S0218348X93001040.

Lenormand, R., E. Touboul, and C. Zarcone. 1988. Numerical models and experiments on immiscible displacement in porous media. J. Fluid Mech. 189, 165–187.

Lenormand, R. 1989. Flow Through Porous Media: Limits of Fractal Patterns, Proc. R. Soc. London, Ser. A 423:159-168.

Løvoll, G., Y. Méheust, K.J. Måløy, E. Aker, and J. Schmittbuhl. 2005. Competition of gravity, capillary and viscous forces during drainage in a two-dimensional porous medium, a pore scale study. Energy 30:861–872.

Løvoll, G., M. Jankov, K.J. Måløy, R. Toussaint, J. Schmittbuhl, G. Schäfer, and Y. Méheust. 2010. Influence of viscous fingering on dynamic saturation-pressure curves in porous media. Transport in Porous Media 86(1):305-324. doi:10.1007/s11242-010-9622-8

Løvoll, G., Y. Méheust, R. Toussaint, J. Schmittbuhl, and K.J. Måløy. 2004. Growth activity

579 during fingering in a porous Hele Shaw cell. Phys. Rev. E 70:026301.
580 doi:10.1103/PhysRevE.70.026301

581 Mandava, S. S., A. Ted Watson, and M.E. Carl. 1990. NMR imaging of saturation during
582 immiscible displacements, AIChE 36(11):1680 – 1686.

583 Méheust, Y., and J. Schmittbuhl. 2000. Flow enhancement of a rough fracture. Geoph. Res. Lett.
584 27: 2989–2992.

585 Méheust Y., and J. Schmittbuhl. 2001. Geometrical heterogeneities and permeability anisotropy
586 of rough fractures. J. Geoph. Res. 106(B2): 2089–2102.

587 Méheust, Y., G. Løvoll, K.J. Måløy, and J. Schmittbuhl. 2002. Interface scaling in a two-
588 dimensional porous medium under combined viscous, gravity, and capillary effects. Phys.
589 Rev. E 66:051603.

590 Méheust, Y., and J. Schmittbuhl. 2003. Scale Effects Related to Flow in Rough Fractures. Pure
591 Appl. Geophys. 160 (2003): 1023-1050.

592 Måløy K.J., J. Feder, and T. Jøssang. 1985. Vicous fingering fractals in porous media, Phys. Rev.
593 Lett. 55:2688-2691

594 Måløy K.J., L. Furuberg, J. Feder, and T. Jøssang. 1992. Dynamics of Slow Drainage in Porous
595 Media. Phys. Rev. Lett. 68:2161-2164

596 Neuville A., R. Toussaint, and J. Schmittbuhl. 2010. Fracture roughness and thermal exchange:
597 A case study at Soultz-sous-forêts. 2010a. Comptes Rendus Geoscience 342(7–8):616–
598 625. doi:10.1016/j.crte.2009.03.006.

599 Neuville A., R. Toussaint, and J. Schmittbuhl. 2010b. Hydro-thermal flows in a self-affine rough
600 fracture. Phys. Rev. E 82:036317. doi:10.1103/Phys- RevE.82.036317.

601 Neuville, A., R. Toussaint, and J. Schmittbuhl. 2011. Hydraulic transmissivity and heat exchange
602 efficiency of rough fractures: a spectral approach, Geoph. J. Int. 186:1064–1072.
603 doi:10.1111/j.1365-246X.2011.05126.x

604 Neuville A., R. Toussaint, J. Schmittbuhl, D. Koehn, and J. Schwarz. 2011. Characterization of
605 major discontinuities from borehole cores of the black consolidated marl formation of
606 Draix (French Alps). Hydrol. Proc., in press, doi: 10.1002/hyp.7984.

607 Neuville A., R. Toussaint, and J. Schmittbuhl. 2011. Fracture aperture reconstruction and
608 determination of hydrological properties: a case study at Draix (French Alps). Hydrol.
609 Proc., in press, doi: 10.1002/hyp.7985.

610 Niebling, M.J., E.G. Flekkøy, K.J. Måløy, and R. Toussaint. 2010. Mixing of a granular layer
611 falling through a fluid. Phys. Rev. E 82:011301. doi:10.1103/PhysRevE.82.011301

612 Niebling, M.J., E.G. Flekkøy, K.J. Måløy, and R. Toussaint. 2010. Sedimentation instabilities:
613 impact of the fluid compressibility and viscosity. Phys. Rev. E 82:051302. doi:
614 10.1103/PhysRevE.82.051302

615 Niemeyer, L., L. Pietronero, and H.J. Wiesmann. 1984. Fractal dimension of dielectric
616 breakdown. Phys. Rev. Lett. 52:1033.

617 Nsir, K., G. Schäfer, R. Di Chiara Roupert, O. Razakarisoa, and R. Toussaint. 2012. Laboratory
618 experiments on DNAPL gravity fingering in water-saturated porous media, Internat. J.
619 Multiphase Flow 40:83-92.

620 Paterson, L., V. Hornof, and G. Neale. 1984. Visualization of a surfactant flood of an oil-
621 saturated porous medium, S.P.E. J, 325-327.

622 Paterson, L., V. Hornof, and G. Neale. 1984. Water fingering into an oil-wet porous medium
623 saturated with oil at connate water saturation. Rev. Inst. Franc. Petr. 39:517-522.

624 Sandnes, B., E.G. Flekkøy, H.A. Knudsen, K.J. Måløy, and H. See. 2011. Patterns and flow in
625 frictional fluid dynamics, Nat. Comm. 2:288, doi:10.1038/comms1289

626 Stokes, J.P., D. A. Weitz, J. P. Gollub, A. Dougherty, M. O. Robbins, P. M. Chaikin, and H. M.
627 Lindsay. 1986. Interfacial Stability of Immiscible Displacement in a Porous Medium.
628 Phys. Rev. Lett. 57:1718

629 Szymczak, P., and A.J.C. Ladd. 2011. Instabilities in the dissolution of a porous matrix. Geoph.
630 Res. Lett. 38, L07403.

631 Tallakstad, K.T., H.A. Knudsen, T. Ramstad, G. Løvoll, K.J. Måløy, R. Toussaint, and E.G.
632 Flekkøy. 2009a. Steady-state two-phase flow in porous media: statistics and transport
633 properties. Phys. Rev. Lett. 102:074502.

634 Tallakstad, K.T., G. Løvoll, H. A. Knudsen, T. Ramstad, E. G. Flekkøy, and K. J. Måløy. 2009b.
635 Steady-state, simultaneous two-phase flow in porous media: An experimental study.
636 Phys. Rev. E 80:036308.

637 Toussaint, R., G. Løvoll, Y. Méheust, K.J. Måløy, and J. Schmittbuhl. 2005. Influence of pore-
638 scale disorder on viscous fingering during drainage. Europhys. Lett. 71: 583.
639 doi:10.1209/epl/i2005-10136-9

640 Varas, G., V. Vidal, and J.C. Geminard. 2011. Morphology of air invasion in an immersed

granular layer. Phys. Rev. E 83(6):061302. doi:10.1103/PhysRevE.83.061302

Vinningland, J.L., Ø Johnsen, E.G. Flekkøy, R. Toussaint, and K.J. Måløy. 2007a. A granular Rayleigh-Taylor instability: experiments and simulations, Phys. Rev. Lett., 99, 048001. doi:10.1103/PhysRevLett.99.048001

Vinningland, J.L., Ø. Johnsen, E.G. Flekkøy, R. Toussaint, and K.J. Måløy. 2007b. Experiments and Simulations of a gravitational granular flow instability, Phys. Rev. E, 76, 051306. doi:10.1103/PhysRevE.76.051306

Vinningland, J.L., Ø. Johnsen, E.G. Flekkøy, R. Toussaint, and K.J. Måløy. 2010. Influence of particle size in Rayleigh Taylor granular flow instability, Phys. Rev. E 81, 041308. doi: 10.1103/PhysRevE.81.041308

Vinningland, J.L., R. Toussaint, M. Niebling, E.G. Flekkøy, and K.J. Måløy. 2012. Family-Viscek scaling of detachment fronts in Granular Rayleigh-Taylor instabilities during sedimentating granular/fluid flows, Eur. Phys. J. S. T.. In press.

Wagner G., A. Birovljev, J. Feder, and T. Jøssang. 1997. Fragmentation and migration of invasion percolation clusters: experiments and simulations, Phys. Rev. E 55:7015-7029.

Weitz, D.A., J. P. Stokes, R. C. Ball, and A. P. Kushnick. 1987. Dynamic Capillary Pressure in Porous Media: Origin of the Viscous-Fingering Length Scale. Phys. Rev. Lett. 59:2967.

Wilkinson D. 1984. Percolation model of immiscible displacement in the presence of buoyancy forces. Phys. Rev. A 30:520-531.

Wilkinson D. 1986. Percolation effects in immiscible displacement, Phys. Rev. A 34:1380-1391.

Wilkinson D., and J.F. Willemsen. 1983. Invasion percolation: a new form of percolation theory. J. Phys. A 16:3365-3376.

Xu, B., Y.C. Yortsos, and D. Salin. 1998. Invasion percolation with viscous forces. Phys. Rev. E 57:739-751.

Yan J., X. Luo, W. Wang, F. Chen, R. Toussaint, J. Schmittbuhl, G. Vasseur, Y. Alan, L. Zhang. 2012. An experimental study of oil secondary migration in a three dimensional porous space. A.A.P.G. Bulletin. In press.

Zimmerman R., and G. Bodvarsson. 1996. Hydraulic conductivity of rock fractures. Trans. Porous Med. 23(1):1–30.

Figure Captions:

Figure 1: Invasion structure of a fluid with a low viscosity (white) into a much more viscous one (dark grey) during drainage in an artificial 2D porous medium of width W and extent L, at three different extraction speeds. The position of the invasion tip is denoted x. Characteristic crossover scales between fractal regimes, λW and a/Ca, separate a straight finger structure, a viscous fingering geometry, and a capillary fingering geometry, down to the pore scale a. The black square of various dimensions in the central figure illustrate the types of boxes used in the box counting measure of the fractal dimension: for boxes of a certain side size *l*, one counts the number of boxes *N(l)* needed to cover the structure. This is done for various sizes, from system size down to pixel size. The scaling of this number as function of the size, $N(l) \sim l^{-D}$ defines the mass fractal dimension *D*. The sizes *W* and *a/Ca* turn out to be the limits of scale-ranges with well defined fractal dimensions: $D = 1.00$ above W, $D_v = 1.60$ between W and a/Ca, and $D_c = 1.83$ below. Modified from Løvoll et al. (2011).

Figure 2: Dependence of the pressure difference between the two phases and the saturation of the invading fluid after removal of the average capillary pressure drop, $\Delta P^* = P_{n.w.} - P_{w.} - \gamma/a$, at different injection speeds. Adapted from Løvoll et al. (2011).

Figure 3: The collapse of the relationship between the reduced pressure difference

690 (between the two phases), $P' = a^2 \Delta P^* / (\gamma L \mathrm{Ca})$, and the reduced saturation of the invading fluid,
691 $S^* = \lambda^{1-D_v} (a/W)^{-2+D_v} \mathrm{Ca}^{D_c - D_v} S_{n.w.}$, at different injection speeds, shows the influence of the
692 structure on the upscaling. Note that plots corresponding to lower Ca values have been rescaled
693 more and therefore appear more noisy. Dashed curve: prediction. Inset: Residual saturation at
694 breakthrough. Adapted from Løvoll et al. (2011).
695